



HAL
open science

Measurement of Liquid Core Length of a Coaxial Two-fluid Spray

D. Li, J K Bothell, T B Morgan, T. Heindel, Nathanaël Machicoane, A. Aliseda, A L Kastengren

► **To cite this version:**

D. Li, J K Bothell, T B Morgan, T. Heindel, Nathanaël Machicoane, et al.. Measurement of Liquid Core Length of a Coaxial Two-fluid Spray. ILASS-Americas 30th Annual Conference on Liquid Atomization and Spray Systems, May 2019, Tempe, United States. hal-02518440

HAL Id: hal-02518440

<https://hal.science/hal-02518440>

Submitted on 25 Mar 2020

HAL is a multi-disciplinary open access archive for the deposit and dissemination of scientific research documents, whether they are published or not. The documents may come from teaching and research institutions in France or abroad, or from public or private research centers.

L'archive ouverte pluridisciplinaire **HAL**, est destinée au dépôt et à la diffusion de documents scientifiques de niveau recherche, publiés ou non, émanant des établissements d'enseignement et de recherche français ou étrangers, des laboratoires publics ou privés.

Measurement of Liquid Core Length of a Coaxial Two-fluid Spray

D. Li*, J. K. Bothell, T. B. Morgan, T. J. Heindel
Center for Multiphase Flow Research and Education,
Department of Mechanical Engineering, Iowa State University,
Ames, IA, 50011, USA

N. Machicoane, A. Aliseda
Department of Mechanical Engineering,
University of Washington,
Seattle, WA, 98195, USA

A. L. Kastengren
Advanced Photon Source,
Argonne National Laboratory,
Lemont, IL, 60439 USA

Abstract

Shadowgraphs, tube-source X-ray radiographs, and synchrotron X-ray radiographs from a coaxial two-fluid spray are analyzed to measure the liquid core length of the spray. Two flow conditions: $Re_l = 1,100$, $Re_g = 21,300$, $We = 40$, and $Re_l = 1,100$, $Re_g = 46,700$, $We = 196$ are investigated. The standard deviation of the fluctuating intensity values are calculated and analyzed to estimate the liquid core length. Additionally, the largest connected domain is used to find an instantaneous breakup position of the spray. The results show that the high standard deviation region is related to the ligament development region, and the instantaneous position identifies ligament formation in the spray.

*Corresponding author: danyuli@iastate.edu

1. Introduction

Liquid sprays are widely used in industrial processes, such as pharmaceutical production, energy conversion, agriculture applications, and spray drying. Characterizing the spray is the first step to precisely control the atomization process and promote the efficient use of a spray in any industrial process. Complete atomization is the result of multiple mechanisms combined in a complex fashion. To simplify the problem, the complete process is divided into individual process steps: (1) internal flow development, (2) primary atomization, and (3) secondary atomization.

Depending on various flow conditions, the liquid disintegration is dominated by different forces acting in or on the liquid. Therefore, various kinds of atomization principles have been used to divide disintegration modes and map breakup regimes, Chigier and Farago [1] developed the first map of breakup regimes for a liquid jet in a coaxial gas stream. Hopfinger [2] improved this map by introducing the momentum ratio between the gas and liquid.

The liquid core length, also known as the breakup length, is taken as the distance from the nozzle exit to the breakup point [3]. Przekwas [4] estimated the liquid core length from conservation of mass fluxes. Lasheras et al. [5] developed a different expression based on continuity of the dynamic pressure at the gas-liquid interface.

In this work, the liquid core length of a coaxial two-fluid spray is measured by using both standard deviation and the instantaneous breakup position. Two flow conditions are investigated: $Re_l = 1,100$, $Re_g = 21,300$, $We = 40$, and $Re_l = 1,100$, $Re_g = 46,700$, $We = 196$. Images from various devices of identical sprays are analyzed, including (1) high-speed shadowgraphy taken at Iowa State University (ISU), (2) high-speed shadowgraphy taken at University of Washington (UW), (3) tube-source X-ray radiography taken at Iowa State University, and (4) high-speed synchrotron X-ray radiography taken at then Advanced Photon Source (APS) at Argonne National Laboratory.

2. Experimental Setup

The two-fluid coaxial atomizer used in this research is an open source canonical atomizer* designed by the University of Washington. As Figure 1 shows, the central axis of the atomizer defines the x-axis (vertical axis) with an origin corresponding to the atomizer exit plane. The spray spanwise coordinate defines the y-axis (horizontal axis) with an origin corresponding to the central axis. The z-axis is the X-ray beam or visible light path direction. To better compare or validate data against that obtain in this study or others published with this system [6-8], the coordinate system (x, y, and z) is nondimensionalized by the characteristic length (the inner diameter of the water outlet, $d_l = 2.1$ mm):

$$X=x/d_l. \quad (1)$$

$$Y=y/d_l. \quad (2)$$

$$Z=z/d_l. \quad (3)$$

The complete experimental flow loop is introduced elsewhere [9]. The tube-source broadband radiographs and shadowgraphs taken at ISU used the identical flow loop as the synchrotron radiographs taken at APS. A similar flow loop was used for the shadowgraphs at UW as well, except that the atomizer was mounted horizontally (rotating 90 degrees around the z-axis) to accommodate their mounting system.

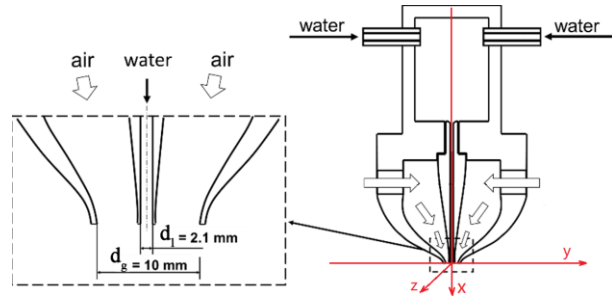


Figure 1. Schematic representation of the two-fluid coaxial atomizer.

Experiments were performed at 25°C, and air was used as the gas phase for the spray. Distilled water was used as the liquid phase for the APS synchrotron X-ray radiographs and the shadowgraphs taken both at ISU and at UW. For the tube-source X-ray radiographs, 20% by mass potassium iodide (KI) was added to increase the contrast in the resulting X-ray images. X-ray radiography is an attenuation-based imaging technique [10], and the image quality is influenced by the intensity of the X-ray source and the material absorptivity. For the APS synchrotron X-ray radiography, the high flux and high energy X-ray beam provides enough intensity that it enables high-speed imaging to show the inner structure of pure water sprays. However, for the ISU tube-source X-ray radiography, the X-ray beam with lower intensity is not sensitive enough to provide clear images of pure water sprays [9]. Therefore, 20% by mass of KI was added for the ISU tube-source X-ray radiography as a contrast enhancement agent. The KI should not significantly influence the surface tension [11] nor enhance beam hardening [12]. Others have also used KI to improve contrast and observed no changes in the flow behavior [12,13]. Shadowgraphy is a light refraction-based technique that captures the interfaces between the liquid and gas, therefore, no additional contrast enhancement methods are required.

The ISU shadowgraphs, UW shadowgraphs, and APS synchrotron X-ray radiographs allow for high-speed imaging and were acquired at speeds of 10,000

* Open-source two-fluid coaxial atomizer: <http://depts.washington.edu/fluidlab/nozzle.shtml>

FPS, 6,000 FPS, and 6,000 FPS, respectively. The ISU tube-source X-ray radiographs were taken at 10 FPS due to the limited transmission speed of the camera. Details about the image acquiring techniques can be found elsewhere [6, 9, 10, 14].

The field of view of the different imaging methods also differ from each other. Theoretically, the ISU tube-source X-ray radiography, and the ISU shadowgraphy provide whole views of the spray. However, limited by the contrast and resolution, the usable region of the ISU tube-source X-ray radiography is limited to approximate 15 mm downstream from the atomizer exit. The UW shadowgraphs show the near-field and middle-field region of the spray. Due to the limitation of the X-ray source size, the APS synchrotron radiography only shows a local view of the spray of approximately 6 mm x 4.5 mm, but were taken at multiple positions in the spray.

The liquid Reynolds number (Re_l) is defined as:

$$Re_l = U_l d_l / \nu_l \quad (4)$$

where U_l is the mean liquid velocity at the nozzle exit, $d_l = 2.1$ mm is the inner diameter of the liquid needle, and ν_l is the kinematic viscosity of water at 25°C. The liquid Reynolds number was fixed in all experiments to $Re_l = 1,100$.

The gas Reynolds number (Re_g) is defined as:

$$Re_g = U_g d_{eff} / \nu_g = U_g \sqrt{d_g^2 - D_l^2} / \nu_g \quad (5)$$

where U_g is the mean gas velocity at the nozzle exit, ν_g is the kinematic viscosity of air at 25°C, and d_{eff} is the gas effective exit diameter of the air stream at the nozzle exit defined as the diameter of a circle with the same exit area found in this study. Note d_g is the inner diameter of the gas nozzle ($d_g = 10$ mm), and D_l is the outer diameter of the liquid needle ($D_l = 2.7$ mm). Two gas Reynolds number in this study are investigated: $Re_g = 21,300$ and $Re_g = 46,700$.

The momentum flux ratio is defined as:

$$M = \rho_g U_g^2 / \rho_l U_l^2 \quad (6)$$

where ρ is the gas and liquid density at 25°C.

The Weber number (We) is defined as:

$$We = \rho_g U_g^2 / \sigma \quad (7)$$

where σ is the interfacial tension.

A summary of all experimental conditions in this study is listed in Table 1.

Re_l	1,100	1,100
Re_g	21,300	46,700
We	40	196
M	6.2	29.7
ISU radiograph	√	√
APS radiograph		√
ISU shadowgraph	√	
UW shadowgraph	√	√

Table 1. Experimental conditions in this study.

3. Data Analysis and Results

3.1 Standard Deviation

Figure 2 shows the spray at $Re_l = 1,100$, $Re_g = 21,300$, $We = 40$. The small Weber number indicates that surface tension plays a dominant role and prevents the liquid jet from breaking up into a uniform spray. As shown in Figure 2a, a few ligaments develop at $X = 2.7$, and break into droplets at $X = 9$. Figure 2b shows the normalized standard deviation (normalized to 0-1) calculated from 600 frames of ISU shadowgraphs. Combining Figure 2a and 2b, it is obvious that the ligament developing region (from $X = 2.7$ to 9) corresponds to the high standard deviation because of the large change in intensity due to the oscillating ligaments. When ligaments breakup, droplet dispersion provides for a more uniform intensity, reducing the standard deviation. In Figure 2b, there is a small region with high standard deviation right below the exit, corresponding to the bright spots inside the liquid jet in Figure 2a. This region results from the light focused by the high curvature surface of the liquid jet, and constantly changed due to surface fluctuations, and hence a high standard deviation in intensity is recorded. Regardless of the impact of light focusing, there is a low standard deviation region in the center of the liquid jet, which indicates a relatively steady flow region inside the liquid core. The high standard deviation area around this region shows the oscillation range of the liquid. Note that for this low We condition, the high standard deviation is caused by the oscillation of the liquid instead of liquid shedding, and this is the reason why the high standard deviation region surrounds the liquid core even near the nozzle exit.

Figure 2c shows a single frame of ISU tube-source X-ray radiograph. The spray details such as ligaments and droplets are blurred out by the long exposure time. The standard deviation distribution of the ISU tube-source X-ray radiographs shows similar characteristics as that of the shadowgraphs, except the deviation on sides are much lower because the fluctuations in the edges of the liquid were not captured due to the low frame rate.

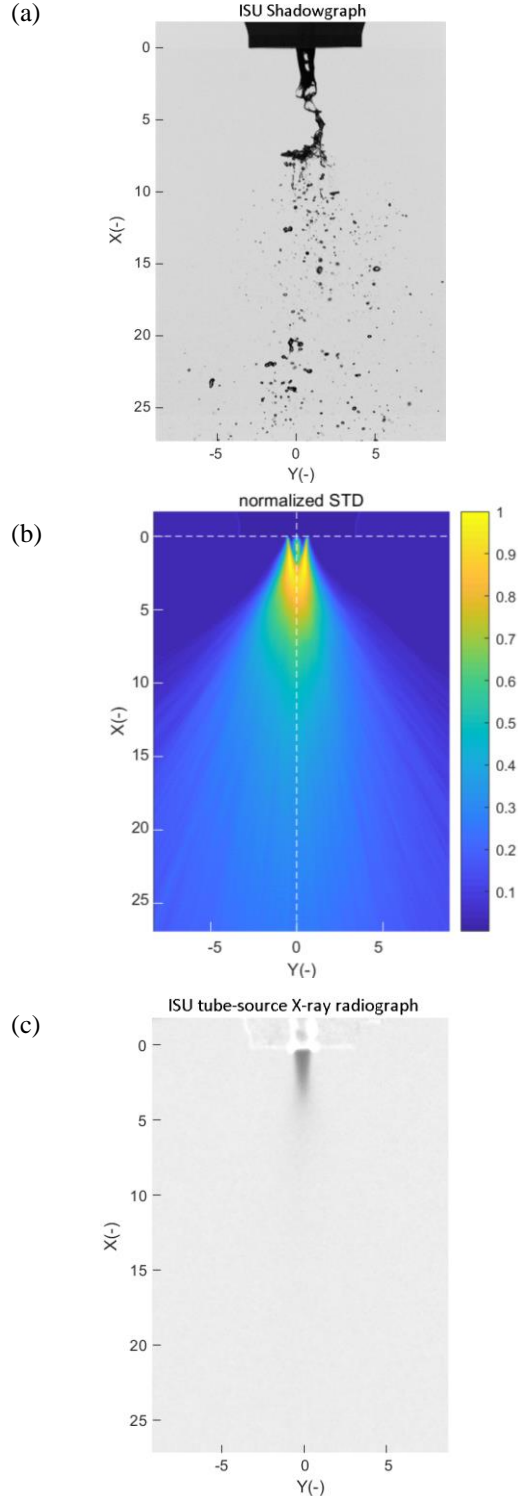


Figure 2. Spray images at $Re_l = 1,100$, $Re_g = 21,300$, $We = 40$: (a) ISU shadowgraph, (b) normalized standard deviation of ISU shadowgraph, and (c) ISU tube-source X-ray radiograph.

The standard deviation along the spray line of symmetry ($Y = 0$) indicates the behavior of the liquid core.

As mentioned above, the high standard deviation of the image intensity is mainly caused by the oscillation of the liquid. The liquid jet stretches and breaks while oscillating at a certain frequency. The position of the highest standard deviation in image intensity corresponds to the position of maximum extent of the oscillating liquid region, where the liquid jet transforms to attached ligaments. Therefore, it is possible to estimate the liquid core length as the position where the standard deviation reaches its maximum.

The plot of normalized standard deviation along $Y = 0$ is shown in Figure 3. The ISU shadowgraph normalized standard deviation shows a secondary peak at $X = 0.7$, corresponding to the bright spots caused by the liquid focusing the light in this region (see for example Figure 2a). UW shadowgraphs were taken with a different backlight and camera system, that shrank the bright spots as Figure 4a shows. Therefore, the UW shadowgraph data reaches the only peak at $X = 2.7$. Both the ISU tube-source X-ray radiograph and UW shadowgraph standard deviation have a maximum at approximate $X = 2.7$, while the maximum of ISU shadowgraph appears at $X = 3.5$. The difference is caused by differing fields of view where the ISU shadowgraphs cover a larger imaging area with an accompanying lower image resolution as the UW shadowgraphs.

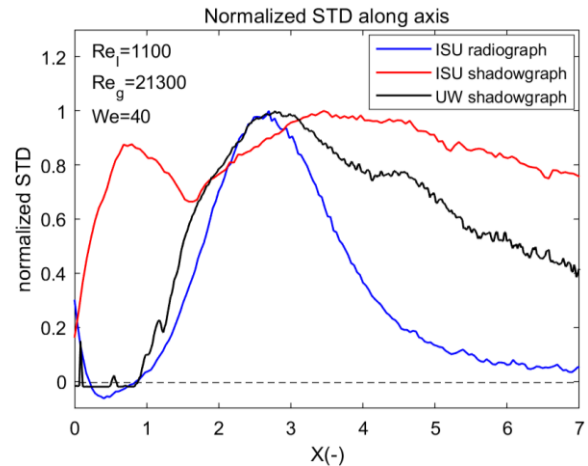


Figure 3. Normalized standard deviation along the X-axis at $Re_l = 1,100$, $Re_g = 21,300$, $We = 40$.

While Figure 3 shows the normalized standard deviation along the nozzle centerline, Figure 4 shows the maximum normalized standard deviation at each X -location at $Re_l = 1,100$, $Re_g = 21,300$, $We = 40$. As mentioned above, shadowgraphs capture the movement of the jet boundary, showing high standard deviation from $X = 0.3$. However, ISU tube-source radiographs can only capture a blurring image of the spray, and the oscillation of the boundary on both sides is ignored. Therefore, the plots based on the ISU tube-source radiographs in Figure 3 and Figure 4 are similar. In Figure 4, three plots all

reach their maximum, as well as an inflection point, at approximate $X = 7$. Therefore, based on the standard deviation, the liquid core length is estimated as $2.7d_l$ for the condition of $We = 40$.

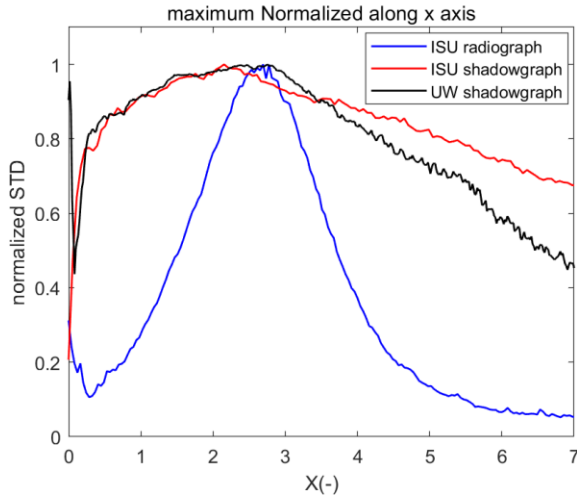


Figure 4. Maximum normalized standard deviation at each X -location at $Re_l = 1,100$, $Re_g = 21,300$, $We = 40$.

Figure 5 shows the spray at the condition of $Re_l = 1,100$, $Re_g = 46,700$, and $We = 196$. In the UW shadowgraph (Figure 5a), ligaments and droplets are reduced in size but increased in number compared to the $We = 40$ condition (Figure 2a). The ligament development region moves from $2.7 \leq X \leq 7$ to $1.6 \leq X \leq 6$ with a large amount of liquid being shed. The APS synchrotron X-ray radiograph (Figure 5b) shows the inner structure of ligaments, and the correspond normalized standard deviation is shown in Figure 5c. The increased standard deviation at the bottom of Figure 5c is caused by the shadow of the chopper wheel when imaging. The standard deviation from the APS imaging shows that the highest fluctuation moved from the central axis to two regions off center because of the smaller and higher frequency fluctuations of the liquid.

Figure 6 shows the maximal standard deviation in each X -plane along the X -axis. Limited by the image size, the APS synchrotron X-ray radiograph data shows only that region available in Figure 5c. The increase at $X = 2.5$ is caused by the chopper wheel as mentioned above. The ISU tube-source radiograph data near the atomizer exit ($X < 0.65$) are discarded due to the influence of accumulated liquid at the atomizer exit. It is hard to determine the maximal standard deviation based on X-ray radiographic data in Figure 6, however, it is obvious that all three plots show a downward trend in the region $X = 1.1$ to 2.5. The UW shadowgraph plot shows similar characteristics as that in Figure 4, which is relatively flat in the region $X = 0.1$ to 1.2, and then declines. The liquid core

length can be estimated by the inflection point of the UW shadowgraph plot at $X = 1.2$.

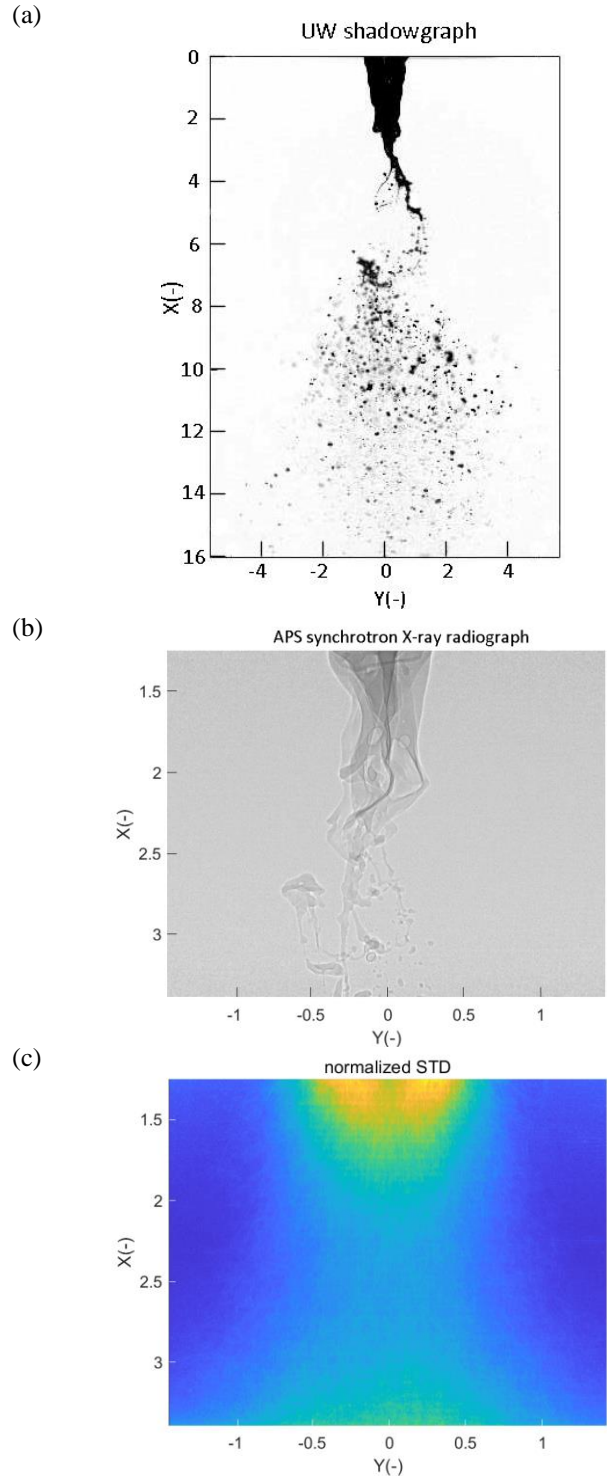


Figure 5. Spray images at $Re_l = 1,100$, $Re_g = 46,700$, $We = 196$: (a) UW shadowgraph, (b) APS synchrotron X-ray radiograph, and (c) normalized standard deviation of the APS synchrotron X-ray radiographs.

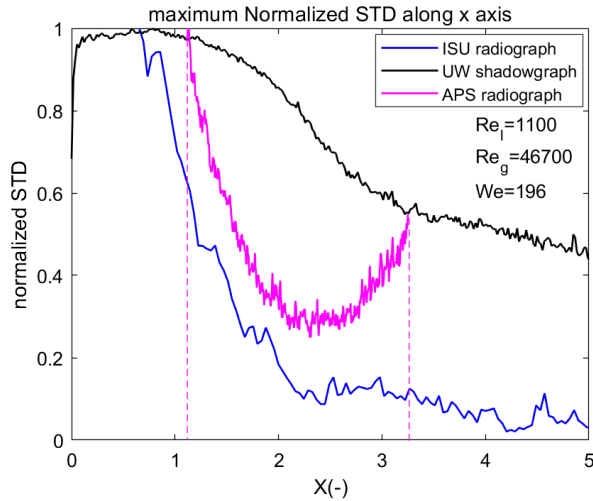


Figure 6. Maximum normalized standard deviation at each X -location at $Re_l = 1,100$, $Re_g = 46,700$, $We = 196$.

In summary, for the two conditions of this work, the large standard deviation region of the spray is qualitatively correlated to the region where ligaments are observed and can be used to estimate the liquid core length.

3.2 Instantaneous Breakup Position

From the high-speed images, including the APS synchrotron radiographs, and the ISU and UW shadowgraphs, it is possible to determine the instantaneous breakup position of the spray by using the maximum connected domain measure. To do this, the image is first converted to a binary image by thresholding. Then the binary image is filtered with a morphological opening with a single structure element size of 4 pixels to suppress the effect of ligaments on determining the connected domain. A 4-connected neighborhood is used to identify the connected components in the binary image, and the entire region is then considered as the liquid core. Finally, the breakup position is defined as the farthest distance along the X -axis that the liquid core can reach. A sample result for a single image is shown in Figure 7. The image processing algorithm is then applied to all high-speed images.

Figure 8a shows the instantaneous breakup position changes with time at $Re_l = 1,100$, $Re_g = 21,300$, and $We = 40$. For the UW shadowgraph plot, some peaks are flattened because the liquid core length goes beyond the field of view. One challenge with instantaneous breakup position tracking is that before a ligament breaks up into droplets, it can have considerable elongation but still be morphologically connected to the liquid core. Therefore, the minimum of the data series, instead of the average, should be considered as the liquid core length. The fluctuation range of the instantaneous breakup position shows the ligament development region instead of the

fluctuation range of liquid core length. The minimum value of $X = 2.8$ corresponds to the location where ligaments start to shed and matches the liquid core length estimated from the standard deviation. The maximum value of $X = 9.1$ corresponds to the location where ligaments breakup into droplets.

To summarize, the fluctuation of the instantaneous breakup position in Figure 8a reflects the development of ligaments. The period of the fluctuation is the cycle for ligaments to develop and breakup. The gentle increasing length with time indicates that the ligament are forming and stretching, and the sharp decline in length indicates ligament shedding.

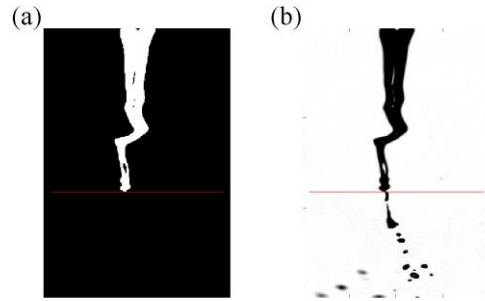


Figure 7. Breakup position identification using a UW shadowgraph at $Re_l = 1,100$, $Re_g = 21,300$, and $We = 40$. (a) Maximum connected domain used to determine the breakup position. (b) The original shadowgraph.

To have a better idea of the ligament shedding frequency, a fast Fourier transform on the instantaneous breakup position was completed, and the result is shown in Figure 8b. The prominent range of the UW shadowgraph data is 36 to 84 Hz, and that of ISU shadowgraph data is 66 to 100 Hz. The ISU shadowgraph data contains more noise due to the lower resolution (but larger field of view).

Figure 9 shows the instantaneous breakup position for $Re_l = 1,100$, $Re_g = 46,700$, and $We = 196$. In Figure 9a, the APS X-ray radiograph data is limited in a band $1.1 \leq X \leq 3.2$ because of the field of view. The fluctuation range of the UW shadowgraph data is $1.8 \leq X \leq 5.5$, which correlates with the ligament developing region ($1.6 \leq X \leq 6$) as mentioned above. The highest FFT peak in the UW shadowgraph data is 85 Hz, which is much larger than that at $We = 40$.

4. Conclusions

Both the large standard deviation region of the spray and the instantaneous breakup position are related to the development of ligaments. The position where the standard deviation reaches the maximum matches the lower limit of the instantaneous breakup position, which can be considered as the liquid core length.

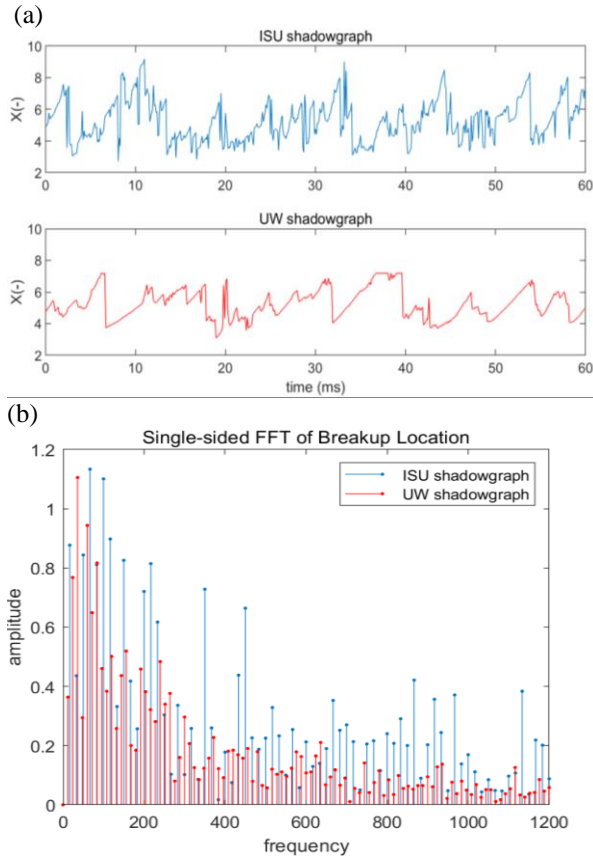


Figure 8. $Re_l = 1,100$, $Re_g = 21,300$, and $We = 40$, showing (a) the instantaneous breakup position tracking, and (b) the single-sided FFT of instantaneous breakup position.

5. Acknowledgements

This work was sponsored by the Office of Naval Research (ONR) as part of the Multidisciplinary University Research Initiatives (MURI) Program, under grant number N00014-16-1-2617. The views and conclusions contained herein are those of the authors only and should not be interpreted as representing those of ONR, the U.S. Navy or the U.S. Government.

A portion of this work was performed at the 7-BM beamline of the Advanced Photon Source, a U.S. Department of Energy (DOE) Office of Science User Facility operated for the DOE Office of Science by Argonne National Laboratory under Contract No. DE-AC02-06CH11357.

The tube-source X-ray facility in this research was funded by the National Science Foundation under award number CTS-0216367 and Iowa State University.

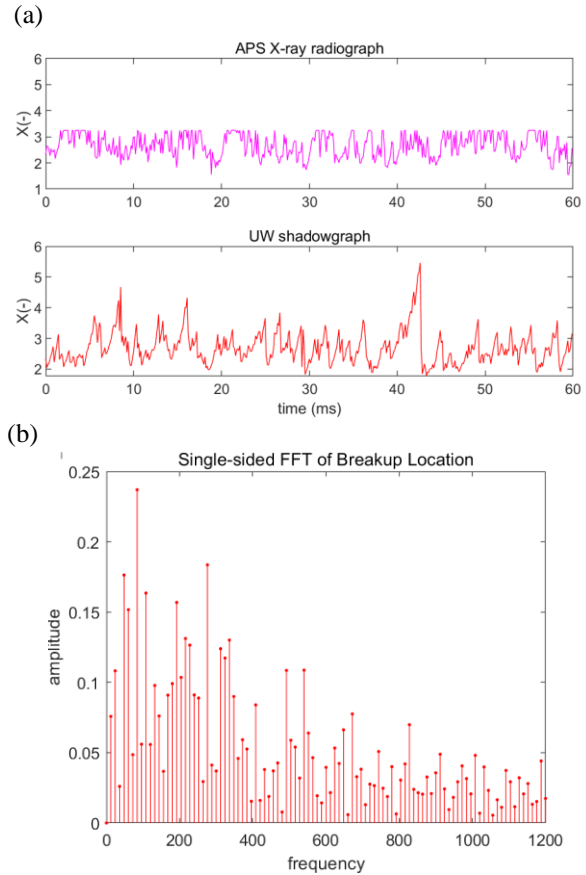


Figure 9. $Re_l = 1,100$, $Re_g = 46,700$, and $We = 196$, showing (a) the instantaneous breakup position tracking, and (b) the single-sided FFT of instantaneous breakup position based on the UW shadowgraphs.

References

1. Chigier, N. and Farago, Z., *Atomization and Sprays*, 2(2):137-153 (1992).
2. Hopfinger, E.J., *Journal of Chemical Engineering of Japan*, 16(4):313-319 (1998).
3. Schwarzkopf, J.D., Michaelides, E. and Crowe, C.T., *Multiphase Flow Handbook, Second Edition*, CRC Press, 2016, p. 1091-1225.
4. Przekwas A.J., *Recent Advances in Spray Combustion: Spray Atomization and Droplet Burning Phenomena*, 166:211-39 (1996).
5. Lasheras, J.C., Villermaux, E. and Hopfinger, E.J., *Journal of Fluid Mechanics*, 357:351-379 (1998).
6. Machicoane, N. and Aliseda, A., *The 29th Annual Conference on Liquid Atomization and Spray Systems, North and South America*, Atlanta, GA, May 2017.
7. Huck, P.D., Machicoane, N., Osuna-Orozco, R., Aliseda, A., *The 14th International Conference on*

- Liquid Atomization and Spray Systems*, Chicago, IL, July 2018.
8. Bothell, J.K., Li, D., Morgan, T.B., Heindel, T.J., Aliseda, A., Machicoane, N., and Kastengren, A.L., *The 14th International Conference on Liquid Atomization and Spray Systems*, Chicago, IL, July 2018.
 9. Li, D., Bothell, J.K., Morgan, T.B., Heindel, T.J., Aliseda, A., Machicoane, N., and Kastengren, A.L., *The 14th International Conference on Liquid Atomization and Spray Systems*, Chicago, IL, July 2018.
 10. Heindel, T.J., *Atomization and Sprays*, 28(11):1029-1059 (2018).
 11. Ali, K. and Bilal, S., *Colloids and Surfaces A: Physicochem. Eng. Aspects*, 337:194-199 (2009).
 12. Halls, B.R., Heindel, T.J., Kastengren, A.L., and Meyer, T.R., *International Journal of Multiphase Flow*, 59:113-120 (2014)
 13. Radke, C.D., Heindel, T.J., and Meyer, T.R., *50th AIAA/ASME/SAE/ASEE Joint Propulsion Conference 2014*, Cleveland, OH, July 2014.
 14. Heindel, T.J., Gray, J.N., and Jensen, T.C., *Flow Measurement and Instrumentation*, 19(2):67-78 (2008).